Apparatus for soft X-ray table-top high harmonic generation

Allan S. Johnson,[1,2] David Wood,[1] Dane R. Austin,[1] Christian Brahms,[1] Andrew Gregory,[1] Konstantin B. Holzner,[1] Sebastian Jarosch,[1] Esben W. Larsen,[1] Susan Parker,[1] Christian Strüber,[1] Peng Ye,[1] John W. G. Tisch,[1] and Jon P. Marangos[1]

[1)] *Blackett Laboratory, Imperial College London, Prince Consort Road, London, SW7 2AZ*

[2)] *ICFO - The Institute of Photonic Sciences, The Barcelona Institute of Science and Technology, Castelldefels, 08860*

(Dated: 25 May 2018)

There has been considerable recent interest in tabletop soft X-ray attosecond sources enabled by the new generation of intense, few-cycle laser sources at operating wavelengths longer than 800 nm. In our recent work (A.S. Johnson *et al.*, Science Advances) we have demonstrated a new regime for the generation of X-ray attosecond pulse in the water window (284-540 eV) by high-harmonic generation, which resulted in soft X-ray fluxes of $\approx 10^9$ photons/s, and a maximum photon energy of 600 eV, an order of magnitude and 50 eV higher, respectively, than previously attained with few-cycle drivers. Here we present the key elements of our apparatus for the generation and detection of soft X-ray high harmonic radiation in the water window. Of critical importance is a differentially pumped gas target capable of supporting the multi-atmospheric pressures required to phase-match the high energy emission while strongly constraining the gas density, suppressing the effects of ionization and absorption outside the interaction region.

PACS numbers: 07.57.-c

I. INTRODUCTION

High harmonic generation (HHG) driven by laser sources with wavelengths beyond 1.5 µm is a promising table-top source of soft X-ray radiation (SXR) for use in time-resolved X-ray absorption experiments and coherent diffractive imaging[1–4]. Of particular interest is the so-called *water window* (WW) region between the carbon K-edge at 284 eV and the oxygen K-edge at 540 eV, in which water is comparatively transparent. Complex organic molecules in solution can thus be probed effectively by addressing the absorption edges of carbon and nitrogen, and in an imaging configuration an X-ray microscope would have extremely high contrast at particular absorption edges combined with nanometer resolution. Recent breakthroughs in SXR harmonic generation were enabled by the use of carrier-envelope phase (CEP) stable few-cycle pulses in the short-wavelength infrared (SWIR, >1.5 µm) to drive the HHG[5], resulting in the first demonstration of attosecond pulses in the water window (284-540 eV)[1,6,7], as well as the first static and transient-absorption spectroscopy measurements with HHG sources in the WW[1,8–10]. Despite these significant advances, challenges remain in regard to increasing both the flux and photon energy of these sources, particularly for harmonics supporting isolated attosecond pulse.

In our recent work we have shown a tenfold improvement in harmonic flux and conversion efficiency for SXR HHG driven by a few-cycle 1.8 µm driving laser, compared to earlier reports using few-cycle lasers. We obtain a flux of $\approx 10^9$ photons/s in the water window along with a harmonic cutoff of 600 eV, a 50 eV extension from previous work reaching well beyond the water window[11]. This dramatic improvement was enabled by moving to a new regime for HHG, which we dubbed the *overdriven* limit, where the harmonic medium is strongly ionized by a driving laser which has a peak intensity much higher than the critical intensity for plasma-defocusing. The generated plasma strongly re-shapes the laser field over a short length, coinciding with a region of high ionization fraction, leading to efficient transient buildup of the harmonic radiation.

SXR harmonic generation comes with additional technical challenges when compared to conventional HHG in the XUV driven by 800 nm lasers. These include the generation of the few-cycle, CEP-stable SWIR pulses and demanding detection requirements for characterizing the SXR emission. Operating in the overdriven regime also places constraints on the high-pressure gas cells required for phase-matching SXR HHG. In particular, because of the strong effects of ionization on the driving laser and the fact that the harmonic radiation builds up transiently over a distance of a few hundred microns, the multi-atmospheric pressures required for phasematching should be confined to as short a longitudinal region as possible, with sub-mbar vacuum maintained elsewhere. Here we present our apparatus for the generation of SXR harmonics in the overdriven regime, which addresses all of these requirements. We first briefly describe the details of the few-cycle, CEP-stable SWIR laser system used to drive HHG, then present a novel differential pumping system with a high-pressure gas cell which allows us to, for the first time, obtain the optimal CEP-dependent water window harmonic flux from helium. This gas-target configuration also fulfils the short-longitudinal extent requirements for overdriven HHG. Finally, we discuss the challenges and construction of an SXR spectrometer optimized for high resolution in the water window. Our system is well suited for the examination and optimization of SXR HHG driven by few-cycle, CEP-stable SWIR pulses, and here we present the first discussion of the unique technical challenges of HHG in this regime.

II. OVERVIEW OF THE APPARATUS

Any system for SXR HHG can be conceptually divided into three stages; driving pulse preparation, high-harmonic generation, and harmonic characterization. As stated above, in our system these stages comprise the generation of a few-cycle, CEP-stable SWIR laser source, HHG in a multi-atmospheric pressure gas target, and detection of the harmonic radiation in an SXR spectrometer; a complete

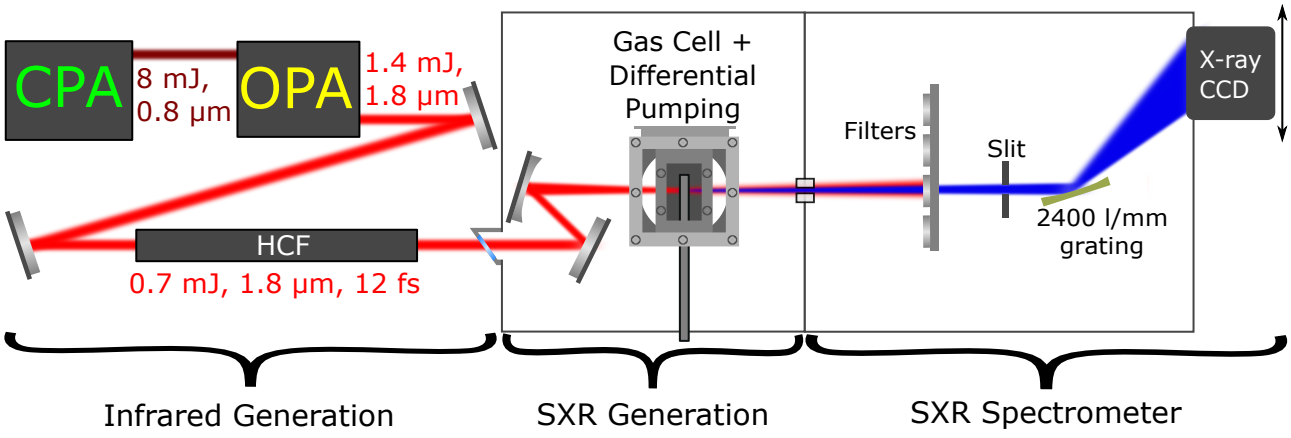


FIG. 1: Summary of the apparatus, divided into infrared pulse generation, SXR harmonic generation, and SXR spectrometer portions. The second two portions take place inside vacuum. Further details are described throughout the main text.

schematic of our apparatus is shown in figure 1. We will discuss each stage in turn, highlighting the differences and challenges as compared to the more conventional process of HHG in the XUV driven by 800 nm lasers.

The generation of few-cycle, CEP-stable sources in the SWIR region has been well described in a variety of works and reviews[12], including our own work on the spatio-temporal characterization of our source[13], so we will only briefly review this first portion of our apparatus. We use the 30 fs, 8 mJ, 800 nm, 1 kHz output of a chirped-pulse amplification laser (KMLabs Red Dragon) to pump a commercial optical parametric amplifier (OPA) (Light Conversion HE:TOPAS) and generate 30 fs, 1.4 mJ idler pulses at 1.75 µm central wavelength. While the idler of such an OPA is passively CEP-stable[14], the CEP is still subject to slow drifts and fluctuations caused by fluctuations in the pump power or by drift inside of the OPA itself. Active feedback is required to obtain long term CEP stability; we control the CEP of the idler by varying the path length between signal and pump inside the final amplification stage of the OPA using a piezo-electric actuated mirror. The idler pulse is spectrally broadened in a hollow capillary, and temporally compressed to two-cycle duration using the anomalous dispersion of a pair of fused silica wedges, with an output pulse energy of 700 µJ. We measure the CEP for our feedback loop using a 2f-3f interferometer taking as input one of the wedge reflections. Using a 2f-3f interferometer relaxes the bandwidth requirement to 2/3 of an octave, which was found to be better compatible with the driving pulse parameters resulting in optimal harmonic generation, without requiring additional broadening before the interferometer[11]. Despite the higher energy requirements of a 2f-3f interferometer, we still obtain single-shot operation. The spatio-temporal characteristics of our pulse are characterized using SEA-F-SPIDER and detailed in Austin *et al.*[13]; extremely good spatio-temporal quality can be achieved with the use of the hollow-capillary compression, and the importance of this property is discussed further in reference 11. The now temporally compressed, CEP-stable idler pulse passes through a Brewster window into the HHG vacuum chamber and is focused using either a spherical mirror or a lens into the HHG target. The focusing optic is mounted on a motorised stage, allowing the location of the laser focus relative to the target to be varied under vacuum. The generated harmonics then pass into a separate spectrometer chamber separated by a 1x4 mm differential pumping slit. We now discuss the details of the generation and characterization portions of the apparatus in the following sections.

III. HIGH-PRESSURE HARMONIC GAS TARGET

A significant challenge to the generation of water window high harmonics is the extremely poor single-emitter efficiency of HHG. Estimates based on time-dependent Schrödinger equation calculations[15] or enhanced strong-field approximation models[16] predict wavelength scaling of between λ^{-5} and λ^{-9}, respectively, where λ is the wavelength of the driving laser. Moving to an 1800 nm driving wavelength from the conventional 800 nm can thus be predicted to cause up to a factor of ≈ 1500 decrease in the single atom yield. However, it is well known that this decrease in single emitter efficiency can be compensated to a significant extent by the phase-matching condition for high energy emission driven by long wavelength sources[3]. It has been shown that the phasematching of HHG under these conditions requires a high pressure nonlinear medium; this high pressure phase matching can increase the number of emitters in the interaction region by one or two orders of magnitude. Thus it is necessary to have a gas target capable of supporting multi-atmospheric pressures in order to maximize the macroscopic harmonic yield. In order to reach the highest harmonic energies in the SXR, this gas must have a high ionization potential, i.e. neon or helium. Neon and helium also minimize re-absorption of the emitted harmonics in the soft X-ray. Using these gases poses a significant technical challenge however, as neon and helium are amongst the hardest gases to pump because of their low relative molecular masses and high heat capacity ratios[17]. For the most efficient operation, we additionally require that the longitudinal extent of the gas target be

short to minimize the effects of re-absorption or driving field distortions (for a full discussion, see Johnson *et al.*[11]). We have thus carefully considered an apparatus in order to maximize the confinement of high pressure helium or neon along the propagation axis.

High harmonic generation is generally performed in one of three geometries: in a gas jet, in a gas cell (long or short compared to the Rayleigh range), or in a capillary[18]. Capillaries have yet to be shown to support isolated attosecond pulse generation, and so we did not consider them for this work. We note that while the following discussion of the difference between the two types of unguided geometries is not relevant to capillary targets, the other aspects of this work - driving pulse preparation, different pumping apparatus, and SXR detection - are relevant, and should be considered for development of capillary-based SXR HHG systems. Returning to those geometries which are known to support isolated attosecond pulse generation, gas jets and gas cells are conceptually very similar; in both cases a reservoir of gas is open to the vacuum chamber through a small orifice. In the case of a gas jet, the laser passes through the plume emitted from the orifice, while in the case of the gas cell two holes are present and the beam passes through the cell itself, in through one hole and out the other. This fundamental similarity between the two geometries allows for easy comparison between the two in terms of the tradeoff between flow rate, achievable target pressure, and target spatial extent, as both can be treated as simple flow of gas through an orifice into vacuum. A conceptual schematic of the two situations is shown in figure 2, which introduces several key quantities.

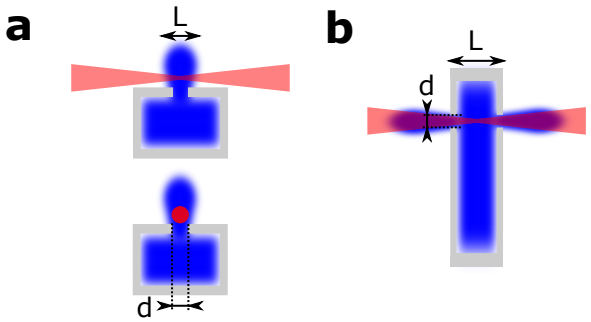


FIG. 2: Comparison of the gas jet (a) and gas cell (b) geometries, showing the different aperture widths d and medium lengths L. The laser is indicated in red, in profile (top) and on-axis (bottom, gas jet only), and the gas distribution is in blue. In both cases the minimum aperture width is set by the waist of the beam.

As mentioned earlier, we require a target as thin as possible in order to suppress unwanted ionization and absorption effects outside the high density central part of the nonlinear medium. This condition naturally favours the geometry of a gas jet as the longitduinal width of a gas jet is largely set by the aperture size d, which can easily be made down to tens of microns. Conversely, a gas cell cannot easily be reduced in size below a few hundred microns without introducing structural problems, and additionally the emitted gas plume will travel along the direction of the incident laser, increasing the effective target length. However, the gas jet geometry presents significant challenges in terms of the attainable interaction gas density. Detailed Monte-Carlo simulations of the flow through short tubes into vacuum are available in the literature[19,20], and show that the gas density drops off very rapidly through a tube and away from the orifice; assuming a laser beam cannot be moved closer than one aperture radius to the orifice, the density at interaction P_{int} is approximately 10% of that at the entrance of the tube (backing pressure P_{b}, $P_{\mathrm{int}} = 0.1P_{\mathrm{b}}$)[19]. This is the case where the jet transverse width has been made to match the waist of the driving pulse. In other words, the attainable interaction density is one-tenth that of the backing pressure for a gas jet. Conversely, for a gas cell, the backing pressure of the orifice directly gives the interaction density ($P_{\mathrm{int}} = P_b$). This means that, for a desired interaction pressure P_{int}, the flow into vacuum for each of the geometries will be given by

$$F_{\mathrm{jet}} \approx f(10P_{\mathrm{int}}) \quad (1)$$

$$F_{\mathrm{cell}} = 2f(P_{\mathrm{int}}) \quad (2)$$

where $f(P_{\mathrm{b}})$ is the flow through an aperture for backing pressure P_{b}. The factor 2 for the cell results from the entrance and exit apertures. Here we have assumed equal aperture sizes for both the cell and gas jet; this is a reasonable assumption provided the longitudinal extent of the cell is small compared to the Rayleigh range, as it is here, ensuring the beam can pass through apertures the size of the beam waist, and thus the minimum aperture size both cases is the beam waist. Because the rate of flow through an aperture scales with the backing pressure as between P_{b} and P_{b}^2, it can be seen that the flow through a gas jet will be much higher than for a gas cell for an equivalent interaction pressure[20,21]. Note that the backing pressure of the system may differ from the backing pressure of the orifice depending on the conductance of the rest of the system, but this does not affect the flow rate scaling of the different targets.

This analysis is supported by the literature; previous work in the water window with gas jets required backing pressures of tens of bars, which in turn required the use of a solenoid valve pulsed jet to maintain reasonable chamber pressures[22]. More recent work has primarily used longer gas cells (several millimeters in extent)[6,23,24], for the superior pressure scaling - the importance of thin targets has only recently been realized[11]. For this reason we have opted to use a thin gas cell as the harmonic target, made up of an 800 µm OD, 720 µm ID stainless steel needle (VWR). The extremely thin (40 µm) stainless steel walls allow for very clean laser drilling of the apertures, but simultaneously show no stress-related problems when filled with over 10 bar of helium. Focusing our few-cycle laser pulse with a 20 cm or 30 cm focal length optic, we drill holes of less than 200 µm diameter into the target, strongly restricting the gas flow out of the needle. Smaller holes can be made at a fixed focal position, but in the interest of allowing scans of the macroscopic generation conditions, specifically focal position, we enlarged the holes by scanning the focus along the propagation direction. A microscope image of the target after several weeks of use is shown in figure 3. The use of extremely thin needles as targets (200 µm diameter) was explored, but these were found to be too prone to damage as the focal spot size

of the laser became comparable to the lateral width of the target. Intermediate values of needle diameters were not explored, but could offer improvements in harmonic flux.

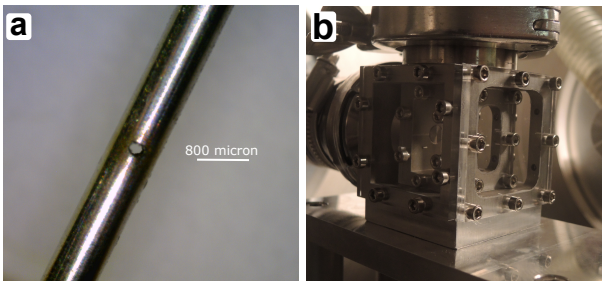


FIG. 3: (a) 800 µm gas needle target with approximately 200 µm laser drilled hole shown. (b) Two-stage differential pumping jacket *in situ*, with bellows leading to pumps.

We additionally designed a differential pumping jacket for the HHG target to allow us to fill the needle target with extremely high pressures (> 10 bar), as previous WW harmonic experiments using helium as the generation medium have seen their maximum flux limited by the attainable backing pressure[22,23]. We used two concentric chambers; the inner chamber was pumped with a screw pump (Oerlikon LV80), whose pumping speed of 80 m^3/h is only weakly dependent on gas species. This is essential for handling the very high flow rate of helium[25] which is difficult for scroll pumps, while oil based pumps introduce significant problems for SXR experiments due to carbon contamination. The outer layer of the jacket is pumped, keeping the pressure outside of the innermost region below 1 mbar, using a small turbomolecular pump (Varian V-81) backed with a seperate roughing pump (Edwards nXDS20iC). The geometry of the target (figure 4) was optimized using a simple model of a Gaussian laser beam passing through clear apertures, and modelling the gas flow from needle apertures as ideal gas jets in the molecular or hydrodynamic limit in which the gas density ρ follows a distribution of $\rho(r,\theta) = \cos^2(\theta)/r^2$ or $\rho(r,\theta) = \cos^4(\theta)/r^2$, respectively[21]. By making all apertures twice as large as the $1/e^2$ width of the Gaussian beam at that point to allow the beam to pass through unobstructed, we can calculate the ideal gas flow through that aperture. We use a Gaussian focus of 60 µm FWHM, closely matching our experimental conditions with a 30 cm focusing mirror; tighter focusing changes the conditions only slightly. We then integrate the gas flux across this aperture, neglecting deviations from the ideal free-space density profile. Figure 4b shows the resulting gas flow from the inner to outer chamber as a function of the inner chamber longitudinal length. The gas flow into the outer chamber of the jacket decreases monotonically as the inner chamber increases in size. Notably, the difference between the two limits of molecular and hydrodynamic flow is relatively small. As the flux decreases monotonically the exact choice of width is somewhat arbitrary: we chose to set the inner chamber size to 26 mm to ensure that the peak pressure inside the outer chamber was around 1 mbar for a 10 bar fill of the needle. This allowed us to safely operate the small turbopump on the outer chamber. The size of the outer chamber was set to be as large as could conveniently fit the geometry of the experiment; we chose a diameter of 50 mm.

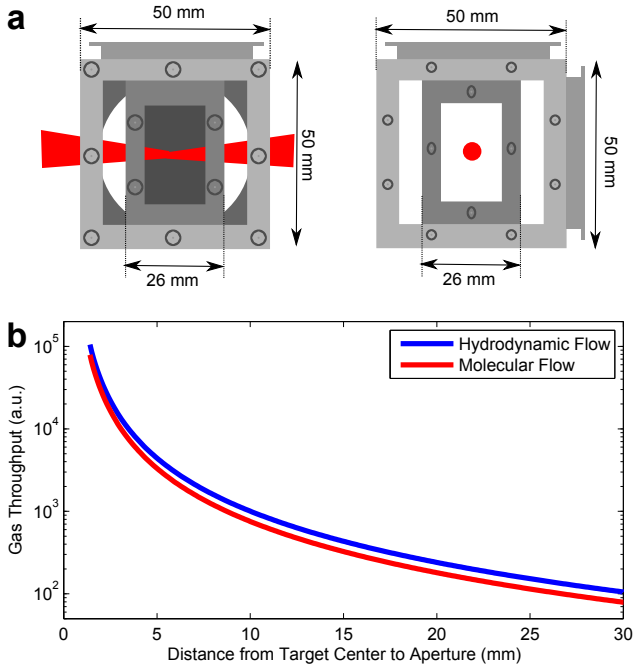


FIG. 4: (a) Schematic of the differential pumping jacket showing the key dimensions, in profile (left) and in the direction of laser propagation (right). The direction of the laser propagation is indicated in red. KF40 bellows attach to the top and back of the jacket for differential pumping. Transparent acrylic windows with small clear apertures of the beam bolt on to the frame to complete the jacket. (b) Gas flux through inner windows as a function of jacket width, with windows adjusted to allow for a 60 µm FWHM Gaussian beam to propagate through unobstructed.

A photo of the resulting chamber is shown in Figure 3b. Large polyurethane windows were used to facilitate easy alignment, while apertures were drilled through the windows to allow the laser and harmonics to pass through unobstructed. These relatively large holes were covered with thin cellophane tape which was then drilled by the laser to ensure an optimally sized aperture. The performance of the jacket and target can be benchmarked by monitoring the chamber pressure as a function of target backing pressure. We measured the backing pressure of the target, the pressure in the inner jacket chamber, the pressure outside the jacket, and the pressure in the adjacent spectrometer chamber separated by a 1x4 mm slit, when backed with He, the hardest noble gas for pumping. The main chamber, approximately a cubic meter in volume, is pumped by two turbomolecular pumps (Pfeiffer TMH1001P 920 l/s, Agilent Turbo-V750 700 l/s), while the approximately 0.5 m^3 spectrometer chamber is pumped by a 550 l/s turbomolecular pump (Agilent Turbo-V550) and a liquid nitrogen filled cold trap. The results are shown in figure 5. Even at the highest backing pressure of 16 bar, all pumps are well within their operating parameters and the spectrometer chamber pressure remains low enough ($< 5 \times 10^{-6}$ mbar) to run a microchannel plate (MCP) detector. In this case we were limited only by the highest pressure that our gas delivery

system could measure and safely deliver (16 bar), and not by the vacuum conditions. The pressure inside the differential pumping can reach pressures of several tens of mbar. While this pressure level could present a problem in the XUV due to re-absorption of the harmonics, absorption cross sections for helium or neon are an order of magnitude lower in the SXR than in the XUV. For high energy harmonic radiation these pressures thus cause negligible absorption over a distance of 25 mm to 50 mm.

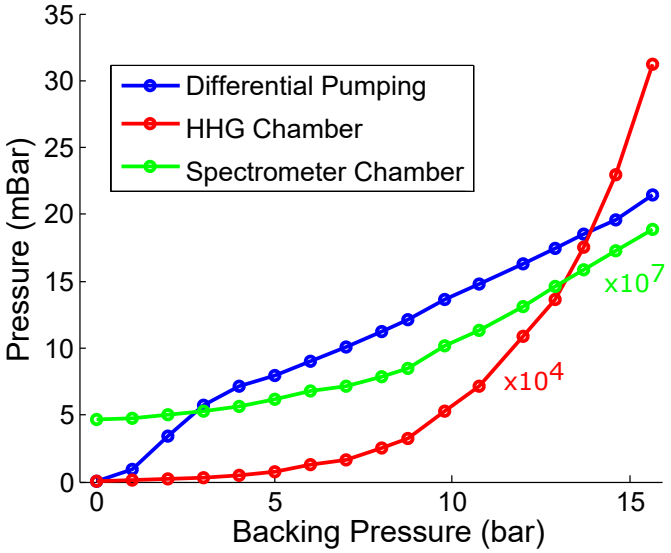


FIG. 5: Pressure of the various sub-chambers as a function of backing pressure in the HHG target. Pressures in the main and spectrometer chambers are scaled by 10^4 and 10^7 respectively for visibility.

IV. SOFT X-RAY SPECTROMETER

After generation in the needle target and differential pumping jacket, the harmonics co-propagate with the fundamental laser beam through an aperture into a spectrometer chamber. The high energies and broad bandwidths of water window HHG present challenges for detection and characterization of the radiation. The extremely broad bandwidths preclude the use of monochromators - to scan over the full bandwidth of an HHG source is prohibitively slow, and prevents single-shot imaging. However to achieve high spectral resolution, i.e. at the sub-eV level in order to observe harmonic structure, across a bandwidth of several hundreds of electron volts simultaneously requires new spectrometer designs. Spectral measurements of HHG often use a transmissive or reflective flat-field grating combined with an imaging detector, and it is this model we have adopted. Conceptually the design of a flat field spectrometer for the soft X-ray is very similar to the XUV, with the only difference being the requirement of a higher line density grating. Practically this poses a large challenge however, as the diffraction efficiency of high line density flat-field gratings is much lower than those appropriate for the XUV, resulting in an up to order of magnitude drop-off in detected signal. This can lead to a poor signal-to-noise (SNR) levels and requires careful implementation.

Conveniently, the availability of VLS gratings with similar working distances but different line spacings (of 1200 l/mm or 2400 l/mm) allows for easy adaptation of one of the most common XUV spectrometer configuration, based around a 1200 l/mm grating and imaging MCP assembly[26], to be adapted to work in the SXR. Our design therefore used a 2400 l/mm VLS grating (Shimadzu 30-003) and with an X-ray CCD detector (Andor Newton SO). When cooled to -100 ^{o}C an X-ray CCD exhibits better thermal and shot signal-to-noise than an MCP and allows for quantitative measurements of harmonic flux through the known quantum efficiency, at the cost of increased sensitivity to visible scattered light. This sensitivity necessitates the use of thin metallics filters at the entrance of the spectrometer to block lower-order harmonics generated in the gas jet which otherwise blind the camera. We used such filters as 100-150 nm thick Al, 250 nm thick Ti, and 200 nm thick Zr free-standing foils (Lebow). The liquid nitrogen cold trap on the spectrometer chamber ensures that there is no condensation on the bare CCD chip when it is cooled.

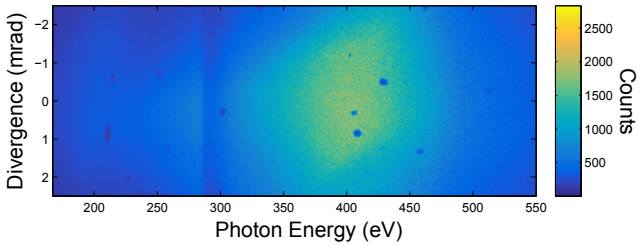


FIG. 6: Spatially resolved harmonic spectrum generated in 2.75 bar of helium using 30 cm focusing. The harmonics show good spatio-spectral structure. Due to the aspect radio of the camera (1:4) we are limited to a relatively narrow range of divergence angles, but the harmonics are sufficiently well collimated to be captured nonetheless. Several dark spots, resulting from contamination on the CCD, are readily visible, and emphasize the importance of the cold trap and general high vacuum conditions to reduce these effects.

The SXR spectrometer layout is as follows: light passes through a filter wheel holding the thin metallic filters necessary for operating the X-ray CCD. The filtered X-rays then pass through a motorized slit with an aperture varying from closed to 6 mm before reflecting off the grating and hitting the X-ray CCD. Because VLS gratings are aberration rather than diffraction limited the best spectrometer resolution requires closing the slit to limit the illumination of the grating[27]; we found a slit size of 250 µm to be sufficient for $\lambda/\Delta\lambda > 500$ operation, both experimentally and through ray-tracing calculations which were used to optimize the dimensions. This leads to significant loss (throughput of the slit was estimated to be around 10%) and so the addition of a re-imaging optic like a toroidal mirror would be an obvious improvement in future implementations. Other important features are that the grating was fully motorized to adjust its position and angle, and that the detector was mounted on a movable flange. We used disc magnet stepping mo-

tors (Portescap P430) cleaned for vacuum operation, along with our own design low vibration Direct Digital Synthesis stepless sin-cosine drive motor controllers. By opening the slit, moving the grating down, and positioning the camera correctly, we could take images of the direct X-ray beam. This is an important feature because of the low diffraction efficiency of the gratings; by passing the beam through an SXR filter (for instance, 250 nm of titanium) we could first coarsely optimize the harmonic flux with the direct beam, before moving back to the more lossy imaging spectrometer configuration. Figure 6 shows a spatially and spectrally resolved harmonic spectrum acquired in our spectrometer. In a single image we can capture harmonic radiation from 150 eV to well above 1 keV, though we have truncated here due to lack of signal outside the range shown in this case. Due to the extremely low noise of the X-ray CCD, the signal-to-noise ratio was primarily limited by lower order harmonics transmitted through the metallic filters, which were found to have microscopic pinholes. These low order harmonics, which are much more intense than the signal, scatter diffusely from the grating and other objects onto the detector, overlapping with the diffraction SXR radiation. Pinholeless filters would further increase the signal-to-noise level. Spectral calibration was performed using the absorption edges of different filters, namely carbon and titanium, which have sharp spectral features. Also visible in the spectrum is a very sharp and strong absorption feature at the carbon K-edge attributable to amorphous carbon contamination; this reaches a maximum of 90% absorption of the SXR radiation at 284 eV, and could be removed through the use of ozone cleaning in future implementations[28]. Dark spots result from contamination on the CCD chip itself, emphasizing the importance of clean vacuum conditions.

V. XANES SPECTRUM AT THE N_2 K-EDGE

The maximum flux obtained integrated across the water window spectral region is $[1.4 \pm 0.4] \times 10^9$ photons/s, or 77 pJ per pulse, one order of magnitude higher than previous water window attosecond sources[11,24,29], though recent work with capillary HHG, which has not yet been shown to support isolated attosecond pulse generation, has achieved higher overall fluxes[30]. Our source is capable of performing X-ray near-edge absorption spectroscopy (XANES) measurements on a timescale shorter than typical synchrotron sources[31]. XANES spectroscopy is much more challenging in terms of flux requirements than extended X-ray absorption spectroscopy (EXAFS) as it demands high spectral resolution and so requires sufficient brightness and stability across sub-eV spetral intervals. For this reasons XANES measurements are a good test for the utility of a source. Figure 7 shows the nitrogen K-edge XANES spectrum of gaseous N_2 obtained using our source. The total acquisition time was 10 min, and various electronic structure peaks are clearly visible, in agreement with the literature[32]. We are also capable of obtaining carbon K-edge absorption spectra in as little as 2 min[8], along with XANES spectra at the sulfur $L_{2,3}$-edge and oxygen K-edge at slightly longer timescales[11]. These acquisition times are already sufficiently short to allow for time-resolved measurements[9], but with the improvements to the spectrometer efficiency discussed above, could be reduced by another two orders of magnitude. This could potentially allow for single-shot acquisition of XANES spectra in the water window with an attosecond pulse, a capability unmatched even by the next-generation of X-ray free electron laser sources.

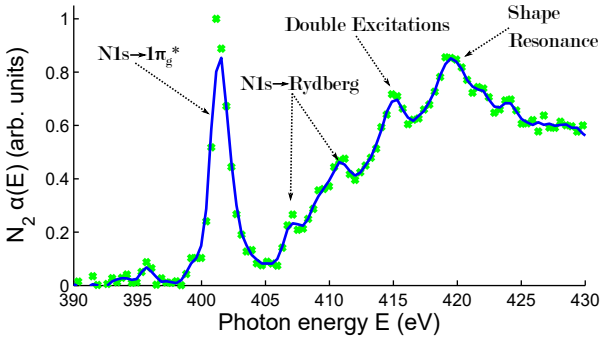


FIG. 7: XANES spectrum of N_2 obtained in ten minutes using our harmonic source. Several electronic structural peaks are visible, especially the pre-edge π^* resonance.

VI. CONCLUSIONS

We have presented an apparatus for the generation of soft X-ray attosecond pulses, especially suited to the overdriven limit. The key elements are the generation of intense, CEP-stable, few-cycle pulses in the SWIR region, a thin, high pressure harmonic gas cell target, and a spectrometer optimized for operation in the soft X-ray. We have described in detail in the design and operation of the gas target and spectrometer. The spectrometer is fundamentally of the same flat-field type as commonly used for XUV harmonics, but with several alterations related to operation in the soft X-ray region highlighted and solutions for overcoming these challenges presented. Most importantly, we have discussed the design and implementation of a thin, high-pressure gas cell and differential pumping setup that has recently allowed us to optimize the SXR harmonic yield in a free-space geometry for the first time[11]. In this paper we have endeavoured to provide a comprehensive guide to implementing a soft X-ray high harmonic generation source in a laboratory, which we hope will enable the proliferation of this remarkable technology beyond the relatively small number of of laboratories which have so far developed this capability.

VII. ACKNOWLEDGEMENTS

This work was supported by EPSRC programme Grant No. EP/I032517/1, ERC ASTEX Project No. 290467, and EPSRC/DSTL MURI EP/N018680/1. A.S.J. and D.A.W. also acknowledge support from Marie Curie ITN EC317232, S.J. acknowledges support from Marie Sklodowska-Curie Grant Agreement No. 641272, and D.R.A. acknowledges support from the Imperial College JRF scheme. A.S.J. acknowledges financial support from the Spanish Ministry of Economy and Competitiveness through the "Severo Ochoa" program for Centres of Excellence in R&D (SEV-2015-0522), from Fundaci Privada Cellex, from the Generalitat de

Catalunya through the CERCA program, and from NSERC PGSD3-454096-2014.
Arduino based motor controller code available upon request from Susan Parker (s.parker@imperial.ac.uk).

[1] Seth L Cousin, F Silva, S Teichmann, Michael Hemmer, B Buades, and Jens Biegert. High-flux table-top soft x-ray source driven by sub-2-cycle, CEP stable, 1.85-μm 1-kHz pulses for carbon K-edge spectroscopy. *Optics Letters*, 39(18):5383, sep 2014.

[2] Lap V Dao, Chris Hall, Hoang L Vu, Khoung B Dinh, Eugenui Balaur, Peter Hannaford, and Trevor A Smith. Phase-matched generation of highly coherent radiation in water window region. *Applied Optics*, 51(18):4240, jun 2012.

[3] Tenio Popmintchev, Ming-Chang Chen, Dimitar Popmintchev, Paul Arpin, Susannah Brown, Skirmantas Alisauskas, Giedrius Andriukaitis, Tadas Balciunas, Oliver D Mücke, Audrius Pugzlys, Andrius Baltuska, Bonggu Shim, Samuel E Schrauth, Alexander Gaeta, Carlos Hernández-García, Luis Plaja, Andreas Becker, Agnieszka a Jaroń-Becker, Margaret M Murnane, and Henry C. Kapteyn. Bright coherent ultrahigh harmonics in the keV x-ray regime from mid-infrared femtosecond lasers. *Science*, 336(6086):1287–91, jun 2012.

[4] Ming-Chang Chen, P. Arpin, T. Popmintchev, M. Gerrity, B. Zhang, M. Seaberg, D. Popmintchev, M. M. Murnane, and Henry C. Kapteyn. Bright, Coherent, Ultrafast Soft X-Ray Harmonics Spanning the Water Window from a Tabletop Light Source. *Physical Review Letters*, 105(17):173901, oct 2010.

[5] Xiaoming Ren, Jie Li, Yanchun Yin, Kun Zhao, Andrew Chew, Yang Wang, Shuyuan Hu, Yan Cheng, Eric Cunningham, Yi Wu, Michael Chini, and Zenghu Chang. Attosecond light sources in the water window. *Journal of Optics*, 20(2):023001, feb 2018.

[6] Nobuhisa Ishii, Keisuke Kaneshima, Kenta Kitano, Teruto Kanai, Shuntaro Watanabe, and Jiro Itatani. Carrier-envelope phase-dependent high harmonic generation in the water window using few-cycle infrared pulses. *Nature Communications*, 5:3331, feb 2014.

[7] S M Teichmann, F Silva, Seth L Cousin, Michael Hemmer, and Jens Biegert. 0.5-keV Soft X-ray attosecond continua. *Nature Communications*, 7(May):11493, may 2016.

[8] Allan S. Johnson, L. Miseikis, D. A. Wood, Dane R. Austin, C. Brahms, S. Jarosch, C. S. Strüber, P. Ye, and J. P. Marangos. Measurement of sulfur L 2,3 and carbon K edge XANES in a polythiophene film using a high harmonic supercontinuum. *Structural Dynamics*, 3(6):062603, nov 2016.

[9] Yoann Pertot, Cédric Schmidt, Mary Matthews, Adrien Chauvet, Martin Huppert, Vit Svoboda, Aaron von Conta, Andres Tehlar, Denitsa Baykusheva, Jean-pierre Wolf, and Hans Jakob Wörner. Time-resolved x-ray absorption spectroscopy with a water window high-harmonic source. *Science*, 355(6322):264–267, jan 2017.

[10] Andrew R Attar, Aditi Bhattacherjee, C. D. Pemmaraju, Kirsten Schnorr, Kristina D. Closser, David Prendergast, and Stephen R. Leone. Femtosecond x-ray spectroscopy of an electrocyclic ring-opening reaction. *Science*, 356(6333):54–59, apr 2017.

[11] Allan S. Johnson, Dane R Austin, David A. Wood, Christian Brahms, Andrew Gregory, Konstantin B. Holzner, Sebastian Jarosch, Esben W. Larsen, Susan Parker, Christian S. Strüber, Peng Ye, John W. G. Tisch, and Jon P. Marangos. High-flux soft x-ray harmonic generation from ionization-shaped few-cycle laser pulses. *Science Advances*, 4(5):eaar3761, may 2018.

[12] Anna Ciriolo, Matteo Negro, Michele Devetta, Eugenio Cinquanta, Davide Faccialà, Aditya Pusala, Sandro De Silvestri, Salvatore Stagira, and Caterina Vozzi. Optical Parametric Amplification Techniques for the Generation of High-Energy Few-Optical-Cycles IR Pulses for Strong Field Applications. *Applied Sciences*, 7(3):265, 2017.

[13] Dane R. Austin, Tobias Witting, Sébastien J. Weber, Peng Ye, Thomas Siegel, Paloma Matía-Hernando, Allan S. Johnson, John W.G. Tisch, and Jonathan P. Marangos. Spatio-temporal characterization of intense few-cycle 2 μm pulses. *Optics Express*, 24(21):24786, oct 2016.

[14] Andrius Baltuška, Takao Fuji, and Takayoshi Kobayashi. Controlling the Carrier-Envelope Phase of Ultrashort Light Pulses with Optical Parametric Amplifiers. *Physical Review Letters*, 88(13):133901, mar 2002.

[15] J. Tate, T. Auguste, H. G. Muller, P. Salières, P. Agostini, and L. F. Dimauro. Scaling of wave-packet dynamics in an intense midinfrared Field. *Physical Review Letters*, 98(1):1–4, 2007.

[16] Dane R. Austin and Jens Biegert. Strong-field approximation for the wavelength scaling of high-harmonic generation. *Physical Review A*, 86(2):023813, aug 2012.

[17] Andrew D Chew. Does pumping Noble gases require special considerations?, 2014.

[18] J.-P. Brichta, M. Wong, J. Bertrand, H.-C. Bandulet, D. Rayner, and V. Bhardwaj. Comparison and real-time monitoring of high-order harmonic generation in different sources. *Physical Review A*, 79(3):033404, mar 2009.

[19] S. Varoutis, D. Valougeorgis, O. Sazhin, and F. Sharipov. Rarefied gas flow through short tubes into vacuum. *Journal of Vacuum Science & Technology A: Vacuum, Surfaces, and Films*, 26(2):228–238, 2008.

[20] S. Varoutis, D. Valougeorgis, and F. Sharipov. Simulation of gas flow through tubes of finite length over the whole range of rarefaction for various pressure drop ratios. *Journal of Vacuum Science & Technology A: Vacuum, Surfaces, and Films*, 27(6):1377, 2009.

[21] David R. Miller. Free Jet Sources. In Giacinto Scoles, editor, *Atomic and Molecular Beam Methods Vol. 1*, chapter 2, pages 14–53. Oxford University Press, New York, 1988.

[22] Eiji J. Takahashi, Tsuneto Kanai, Kenichi L. Ishikawa, Yasuo Nabekawa, and Katsumi Midorikawa. Coherent Water Window X Ray by Phase-Matched High-Order Harmonic Generation in Neutral Media. *Physical Review Letters*, 101(25):253901, dec 2008.

[23] Stephan M Teichmann, Francisco Silva, Seth L Cousin, and Jens Biegert. Importance of intensity-to-phase coupling for water-window high-order-harmonic generation with few-cycle pulses. *Physical Review A*, 91(6):063817, jun 2015.

[24] Cédric Schmidt, Yoann Pertot, Tadas Balciunas, Kristina Zinchenko, Mary Matthews, Hans Jakob Wörner, and Jean-Pierre Wolf. High-order harmonic source spanning up to the oxygen K-edge based on filamentation pulse compression. *Optics Express*, 26(9):11834, apr 2018.

[25] R. Arztmann. Experience with dry running vacuum pumps in helium service. *AIP Conference Proceedings*, 985:316–322, 2008.

[26] Felicity Mcgrath, Allan S Johnson, Dane R Austin, Peter Hawkins, David Wood, Lukas Miseikis, R Emma, Marta Castillejo, Ricardo Torres, Susan Parker, Thomas Siegel, Jon P Marangos, Felicity Mcgrath, Allan S Johnson, Dane R Austin, Peter Hawkins, David Wood, Thomas Siegel, and Jon P Marangos. An apparatus for quantitative high-harmonic generation spectroscopy in molecular vapours An apparatus for quantitative high-harmonic generation spectroscopy in molecular vapours. *Review of Scientific Instruments*, 103108(88), 2017.

[27] David Neely. Private Communication. Technical report, 2018.

[28] Mukund Kumar, Mohd. Hussain Modi, Himanshu Singhal, S Sendhil Raja, Juzer Ali Chakera, Raj Kumar Gupta, Prasad Anant Naik, Gyanendra Singh Lodha, and Parshotam Dass Gupta. Restoration of absolute diffraction efficiency and blaze angle of carbon contaminated gratings by ultraviolet cleaning. *Appl. Opt.*, 52(8):1725–1730, 2013.

[29] Bárbara Buades, Dooshaye Moonshiram, Themistoklis P. H. Sidiropoulos, Iker León, Peter Schmidt, Irina Pi, Nicola Di Palo, Seth L. Cousin, Antonio Picón, Frank Koppens, and Jens Biegert. Dispersive soft x-ray absorption fine-structure spectroscopy in graphite with an attosecond pulse. *Optica*, 5(5):502, may 2018.

[30] Dimitar Popmintchev, Benjamin R. Galloway, Ming-Chang Chen, Franklin Dollar, Christopher A. Mancuso, Amelia Hankla, Luis Miaja-Avila, Galen O'Neil, Justin M. Shaw, Guangyu Fan, Skirmantas Ališauskas, Giedrius Andriukaitis, Tadas Balčiunas, Oliver D. Mücke, Audrius Pugzlys, Andrius Baltuška, Henry C. Kapteyn, Tenio Popmintchev, and Margaret M. Murnane. Near- and Extended-Edge X-Ray-Absorption Fine-Structure Spectroscopy Using Ultrafast Coherent High-Order Harmonic Supercontinua. *Physical Review Letters*, 120(9):093002, 2018.

[31] Nobuhisa Ishii, Keisuke Kaneshima, Teruto Kanai, Shuntaro Watanabe, and Jiro Itatani. Generation of sub-two-cycle millijoule infrared pulses in an optical parametric chirped-pulse amplifier and their application to soft x-ray absorption spectroscopy with high-flux high harmonics. *Journal of Optics*, 20(1):014003, jan 2018.

[32] C. T. Chen, Y. Ma, and F. Sette. K-shell photoabsorption of the N2 molecule. *Physical Review A*, 40(11):6737–6740, 1989.